Structural Engineering and Mechanics, Vol. 4, No. 5 (1996) 569-586
DOI: http://dx.doi.org/10.12989/sem.1996.4.5.569

Three dimensional non-conforming 8-node solid elements with rotational degrees of freedom

Chang-Koon Choi† and Keun-Young Chung‡

Department of Civil Engineering, Korea Advanced Institute of Science and Technology, Taejeon 305-701, Korea.

Nam-Ho Lee‡†

Korea Power Engineering Company, Inc., Yongin 449-910, Korea

Abstract. A new three-dimensional 8-node solid element with rotational degrees of freedom is presented. The proposed element is established by adding rotational degrees of freedom to the basic 8-node solid element. Thus the element has three translations and three rotational degrees of freedom per node. The corner rotations are introduced by transforming the hierarchical mid-edge displacements which are parabolic shape along an edge. The derivation of the element is based on the mixed variational principles in which the rotations are introduced as independent variables. Several types of non-conforming modes are selectively added to the displacement fields to obtain a series of improved elements. The resulting elements do not have the spurious zero energy modes and Poisson's ratio locking and pass patch test. Numerical examples show that presented non-conforming solid elements with rotational degrees of freedom show good performance even in the highly distorted meshes.

Key words: 8-node solid element; hierarchical mid-edge displacement; rotational degrees of freedom; corner rotations; mixed variational principles; non-conforming modes.

1. Introduction

The need for solid elements with rotational degrees of freedom has arisen in many practical engineering problems. Element with rotational degrees of freedom are advantageously used in many structural analysis problems. When spatial beams and shell elements are connected with solid elements, six degrees of freedom - three displacements and three rotations are required at each node and there will be no problems regarding discrepancy in the number of nodal degrees of freedom if solid elements have rotational degrees of freedom. Thus this solid element with rotational degrees of freedom will provide versatile tool in the analysis of engineering problems. As a result, the interest of the engineering community in the element with rotational degrees of freedom was manifested lately by a series of papers on the subject (Hughes and Brezzi 1989, Ibrahimbegovic and Wilson 1991, Choi and Lee 1995, Allman 1984, 1988, Yunus *et al.* 1989

† Professor
‡ Graduate Student
‡† Senior Researcher

and 1991, Pawlak *et al.* 1991, Cook 1986, 1987, MacNeal and Harder 1988, Choi and Chung 1995).

The main advantages of developing the solid element with rotational degrees of freedom are: (1) To improve the element performance while avoiding the use of higher order elements which have mid-edge nodes and have complexity to define element geometry. (2) To simplify the modeling of connection between solid and beams and/or shells, which have rotational degrees of freedom. (3) To represent an alternative approach to solve thick shell problems using solid elements with rotational degrees of freedom.

Lots of efforts have been made to define a corner rotation of a solid element. A three-dimensional continuum mechanics problem can be formulated with the variational principle which employs an independent rotation field. In this formulation, first given by Reissner 1965, the symmetry of the stress tensor is not enforced *a priori*. The skew-symmetric part of the stress tensor appears as a Lagrange multiplier for enforcing the equality of the independent rotation field to the skew-symmetric part of displacement gradient. Hughes and Brezzi (1989) have extended this Reissner's formulation by recognizing the instability of discrete approximations and suggested a way in which the discrete approximation could be stabilized. These developments are in a sharp contrast with the previous works on elements with drilling degrees of freedom (Allman 1984 and 1988, Cook 1987, MacNeal and Harder 1988). The finite elements based on the extended Reissner's formulation have been presented in a number of recent works by several researchers (Ibrahimbegovic and Wilson 1991, Choi and Lee 1995, Allman 1984, Choi and Chung 1995). These elements are built on a special hierarchical displacement field. In developing 8-node solid element, Ibrahimbegovic, *et al.* 1991 extended the applications of Hughes and Brezzi's work to combine with serendipity shape functions for the mid-edge nodes of the 20-node element.

In this paper, these previous works are utilized as bases for developing a new non-conforming 8-node solid element with rotational degrees of freedom. A mixed-type variational formulation in which the rotational field is interpolated independently was used with the skew-symmetric part of the stress tensor. The proposed elements are built on a special hierarchical interpolation of displacement field and possess six degrees of freedom per node. By the use of additional non-conforming modes in the element, performance of the element is much improved and the Poisson's ratio locking phenomena is eliminated. Numerical tests are carried out to evaluate the validity of new formulation.

2. Variational formulation

2.1. Strong form of the boundary value problem

In the given domain Ω occupied by a body (See Fig. 1), the stress tensor σ is treated as a dependent variable which is assumed as non-symmetric. Additional dependent variables concerned are displacement vector $\boldsymbol{u}$, and a skew-symmetric tensor $\boldsymbol{\psi}$ which represents the rotation (See Fig. 2). Utilizing the standard indicial notation, the boundary value problem under consideration is expressed as;

$$\sigma_{ji,j}+f_i=0 \tag{1}$$

$$skew\ \sigma_{ij}=0 \tag{2}$$

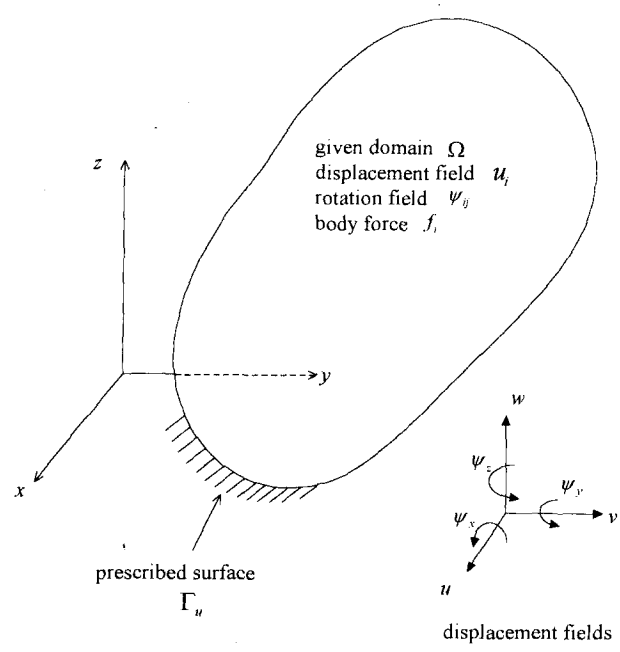

Fig. 1 Boundary value problem.

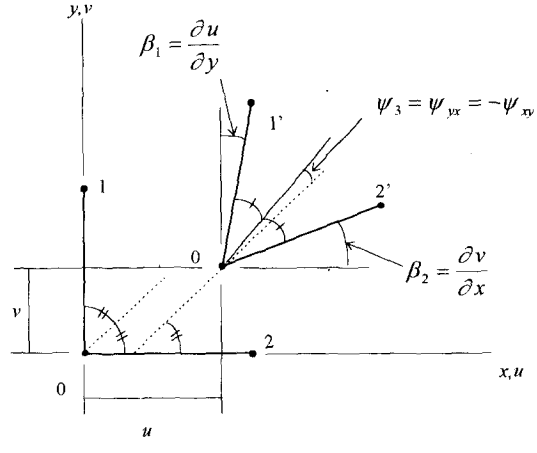

Fig. 2 Definition of rotation field.

$$\psi_{ij} = skew\ u_{i,j} \tag{3}$$

$$symm\ \sigma_{ij} = C_{ijkl}\ symm\ u_{k,l} \tag{4}$$

where Eqs. (1) to (4) are, respectively, the equilibrium equations, the symmetric conditions for stress tensor $\boldsymbol{\sigma}$, the definition of the skew-symmetric rotation tensor $\boldsymbol{\psi}$ in terms of displacement

gradient, and the constitutive equations.

For the isotropic elasticity, the constitutive modulus tensor C_{ijkl} has the form

$$C_{ijkl}=\lambda\,\delta_{ij}\,\delta_{kl}+\mu(\delta_{ik}\,\delta_{jl}+\delta_{il}\,\delta_{jk}) \tag{5}$$

where λ and μ are Lamê's constants and δ_{ij} is Kronecker delta.

2.2. Variational functional

Reissner's variational principle for the boundary value problem Eqs. (1) to (4) leads to a formulation which is inappropriate for numerical applications and inconvenient for the interpolation fields. (Hughes and Brezzi 1989, Ibrahimbegovic and Wilson 1991).

Hughes and Brezzi (1989) modified the variational problem of Reissner by adding the term

$$-\frac{1}{2}\gamma^{-1}\int_{\Omega^e}|skew\ \boldsymbol{\sigma}|^2 d\Omega \tag{6}$$

in order to preserve the stability of the discrete problem. For the isotropic elasticity problems and the Dirichlet boundary value problems, it was suggested that γ be taken as the shear modulus value, i.e. $\gamma=\mu$ (Hughes and Brezzi 1989, Ibrahimbegovic and Wilson 1991). Various variational formulations can be developed by eliminating fields through the use of Euler-Lagrange equations. If the symmetric components of stress are eliminated using the constitutive Eq. (4) for example, the modified variational formulation is given as a Mixed type formulation.

$$\begin{aligned}\Pi_\gamma^e(\boldsymbol{u},\ \boldsymbol{\psi},\ skew\ \boldsymbol{\sigma})=&\frac{1}{2}\int_{\Omega^e}(symm\ \nabla\boldsymbol{u})\cdot\boldsymbol{C}\cdot(symm\ \nabla\boldsymbol{u})\,d\Omega+\int_{\Omega^e}skew\,\boldsymbol{\sigma}^T\cdot(skew\ \nabla\boldsymbol{u}-\boldsymbol{\psi})\,d\Omega\\&-\frac{1}{2}\gamma^{-1}\int_{\Omega^e}|skew\,\boldsymbol{\sigma}|^2 d\Omega-\int_{\Omega^e}\boldsymbol{u}\cdot\boldsymbol{f}\,d\Omega\end{aligned} \tag{7}$$

It is possible to eliminate the skew-symmetric part of stress tensor, denoted as *skew* $\boldsymbol{\sigma}$, by substituting the Euler-Lagrange equation of *skew* $\boldsymbol{\sigma}$

$$\gamma^{-1}\,skew\,\boldsymbol{\sigma}=skew\,\nabla\boldsymbol{u}-\boldsymbol{\psi} \tag{8}$$

into Eq. (7) to obtain the formulation based entirely on kinematic variables, namely, displacements and rotations.

$$\widetilde{\Pi}_\gamma^e(\boldsymbol{u},\ \boldsymbol{\psi})=\frac{1}{2}\int_{\Omega^e}(symm\ \nabla\boldsymbol{u})\cdot\boldsymbol{C}\cdot(symm\ \nabla\boldsymbol{u})\,d\Omega+\frac{1}{2}\gamma\int_{\Omega^e}|skew\ \nabla\boldsymbol{u}-\boldsymbol{\psi}|^2 d\Omega-\int_{\Omega^e}\boldsymbol{u}\cdot\boldsymbol{f}\,d\Omega \tag{9}$$

3. Finite element interpolation

The symmetric tensors and skew-symmetric tensors in variational functional can be rewritten in a standard vector form as

$$symm\,\nabla\boldsymbol{u}^h=\langle u_{1,1}^h\ \ u_{2,2}^h\ \ u_{3,3}^h\ \ u_{1,2}^h+u_{2,1}^h\ \ u_{2,3}^h+u_{3,2}^h\ \ u_{1,3}^h+u_{3,1}^h\rangle^T \tag{10}$$

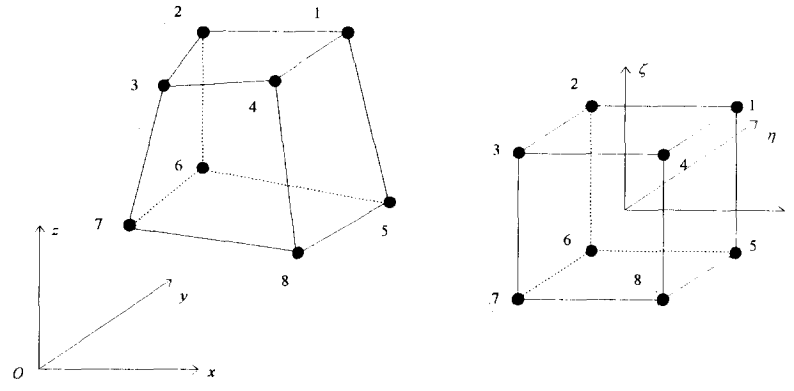

(a) 8-node solid element in physical coordinate system

(b) parent element in natural coordinates system

Fig. 3 Eight-node solid element with rotational degrees of freedom.

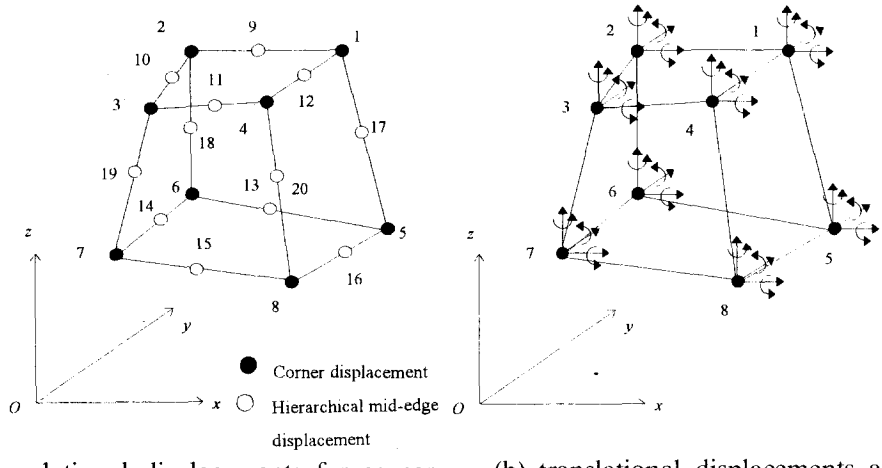

(a) translational displacements for corner nodes and mid-edges

(b) translational displacements and rotation for corner nodes

Fig. 4 Introduction of corner rotations by hierarchical mid-edge displacement.

$$\boldsymbol{\psi}^h = \langle \psi_1^h \;\; \psi_2^h \;\; \psi_3^h \rangle^T \tag{11}$$

$$skew\ \nabla \boldsymbol{u}^h = \frac{1}{2}\langle u_{3,2}^h - u_{2,3}^h \;\; u_{1,3}^h - u_{3,1}^h \;\; u_{2,1}^h - u_{1,2}^h \rangle^T \tag{12}$$

The configuration of the 8-node solid element is defined by (See Fig. 3)

$$\boldsymbol{x}^h = \sum_{I=1}^{8} N_I^c(\xi,\ \eta,\ \zeta)\boldsymbol{x}_I^c \tag{13}$$

where $\boldsymbol{x}^h$ represents global coordinates and N_I^c are the shape functions for corner nodes given as

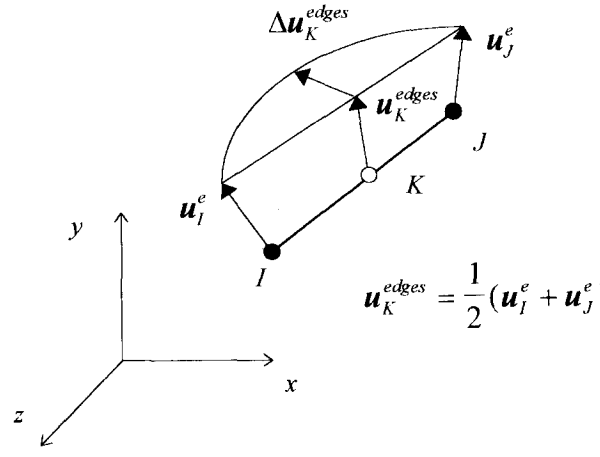

Fig. 5 Hierarchical interpolation of edge displacements.

$$N_I^c(\xi,\ \eta,\ \zeta)=\frac{1}{8}(1+\xi\xi_I)(1+\eta\eta_I)(1+\zeta\zeta_I) \quad I=1,\ 2,\ \cdots,\ 8 \tag{14}$$

The non-conventional interpolation for the displacements field of 8-node solid element is derived from the translational displacements of the eight nodal displacements and twelve hierarchical mid-edge displacements. (see Fig. 4 and 5)

$$\begin{pmatrix} u_1^h \\ u_2^h \\ u_3^h \end{pmatrix} = \boldsymbol{u}^h = \sum_{I=1}^{8} N_I^c(\xi,\ \eta,\ \zeta)\,\boldsymbol{u}_I^c + \sum_{k=9}^{20} N_k^{edges}(\xi,\ \eta,\ \zeta)\,\Delta\boldsymbol{u}_K^{edges} \tag{15}$$

where $\Delta\boldsymbol{u}_K^{edges}$ are the hierarchical displacements added to the conventional nodal displacements and N_K^{edges} are the hierarchical shape functions given as

$$N_K^{edges}(\xi,\ \eta,\ \zeta)=\frac{1}{4}(1-\xi^2)(1+\eta\eta_K)(1+\zeta\zeta_K) \quad K=9,\ 11,\ 13,\ 15 \tag{16}$$

$$N_K^{edges}(\xi,\ \eta,\ \zeta)=\frac{1}{4}(1+\xi\xi_K)(1-\eta^2)(1+\zeta\zeta_K) \quad K=10,\ 12,\ 14,\ 16 \tag{17}$$

$$N_K^{edges}(\xi,\ \eta,\ \zeta)=\frac{1}{4}(1+\xi\xi_K)(1+\eta\eta_K)(1-\zeta^2) \quad K=17,\ 18,\ 19,\ 20 \tag{18}$$

These hierarchical shape functions are parabolic along the edge joining the adjacent two nodes (See Fig. 5). The mid-edge hierarchical displacement components perpendicular to element edges can be replaced by nodal drilling rotations $\boldsymbol{\psi}_I^c$. Edge-normal displacement component can be expressed by corner nodal rotations $\boldsymbol{\psi}_I^c$ and $\boldsymbol{\psi}_J^c$. This transformation is carried out by the projection of displacement $\Delta\boldsymbol{u}_K^{edges}$ onto xy, yz and zx-plane, respectively (See Fig. 6). Thus

$$(\Delta\boldsymbol{u}_K^{edges})_{xy\text{-}plane}^{edge\text{-}normal} = \frac{1}{8}\begin{Bmatrix} -y_J^c+y_I^c \\ x_J^c-x_I^c \\ 0 \end{Bmatrix}(\boldsymbol{\psi}_{Iz}^c - \boldsymbol{\psi}_{Jz}^c) \tag{19}$$

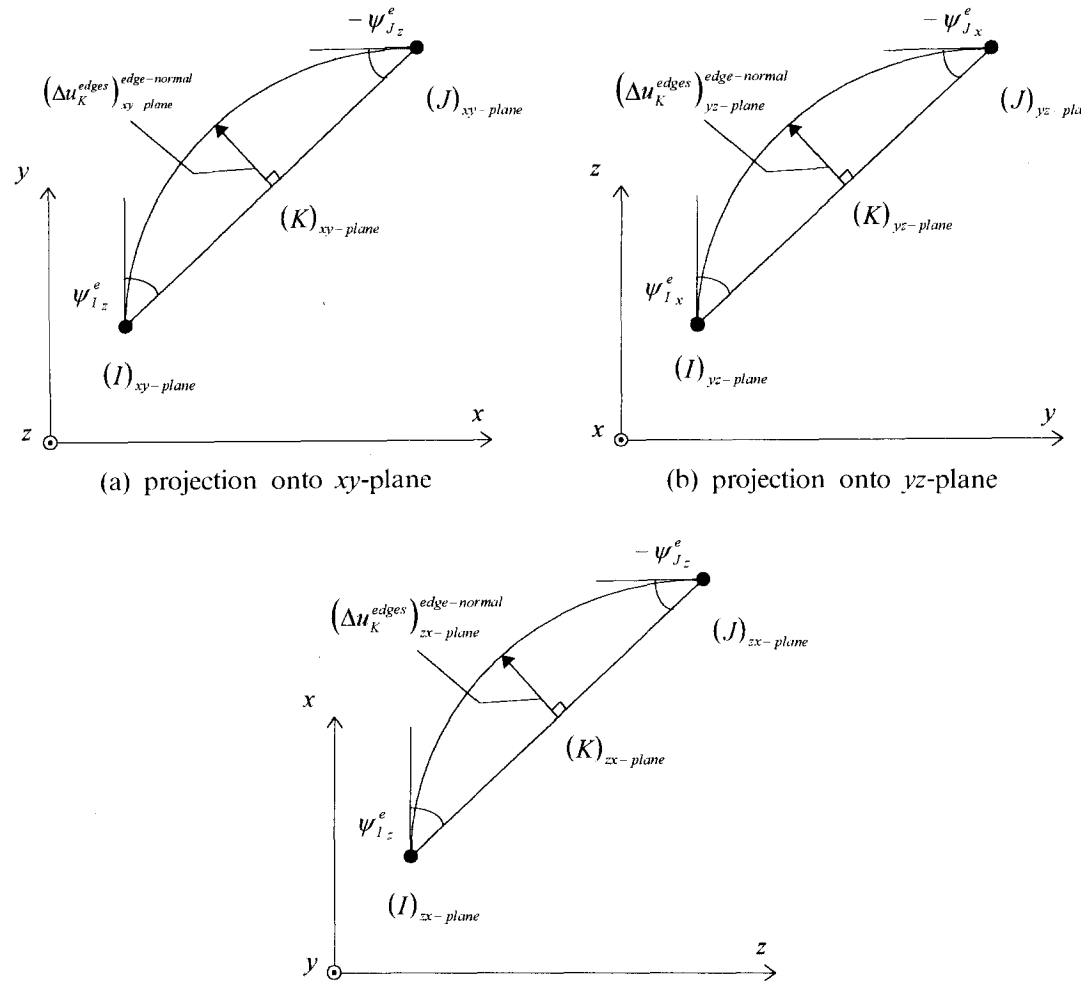

(a) projection onto *xy*-plane

(b) projection onto *yz*-plane

(c) projection onto *zx*-plane

Fig. 6 Hierarchical edge-normal displacements represented by corner rotation which can be obtained from projection onto plane.

$$(\Delta \boldsymbol{u}_K{}^{edges})^{edge\text{-}normal}_{yz\text{-}plane} = \frac{1}{8}\begin{Bmatrix} 0 \\ -z_J^e + z_I^e \\ y_J^e - y_I^e \end{Bmatrix} (\boldsymbol{\psi}_{Ix}^e - \boldsymbol{\psi}_{Jx}^e) \tag{20}$$

$$(\Delta \boldsymbol{u}_K{}^{edges})^{edge\text{-}normal}_{zx\text{-}plane} = \frac{1}{8}\begin{Bmatrix} z_J^e - z_I^e \\ 0 \\ -x_J^e + x_I^e \end{Bmatrix} (\boldsymbol{\psi}_{Iy}^e - \boldsymbol{\psi}_{Jy}^e) \tag{21}$$

It is not possible to properly express the edge-tangential displacement by the nodal drilling rotations. This edge-tangential displacement was neglected in the previous studies (Ibrahimbegovic 1991, Yunus, *et al.* 1989, 1991). In this paper, however, the edge-tangential displacement component is treated as the amplitude of non-conforming modes and included in the element formulation

(Choi and Chung 1995), i.e., $(\Delta\tilde{u}_K^{edges})_{tangential}$ for the typical edge *I-J* shown in Fig. 5, the displacement at the mid-edge point *K*, which is not a physical node, can be written as

$$\Delta \boldsymbol{u}_K^{edges} = \boldsymbol{T}_{IJ}^e(\boldsymbol{\psi}_I^e - \boldsymbol{\psi}_J^e) + \hat{\boldsymbol{l}}_{IJ}^{edges}(\Delta\tilde{u}_K^{edges})_{tangentail} \tag{22}$$

$$\boldsymbol{T}_{IJ}^e = \frac{1}{8}\begin{bmatrix} 0 & z_J^e - z_I^e & -y_J^e + y_I^e \\ -z_J^e + z_I^e & 0 & x_J^e - x_I^e \\ y_J^e - y_I^e & -x_J^e + x_I^e & 0 \end{bmatrix} \tag{23}$$

$$\hat{\boldsymbol{l}}_{IJ}^{edges} = \frac{1}{l_{IJ}^{edges}} \langle x_J^e - x_I^e \;\; y_J^e - y_I^e \;\; z_J^e - z_I^e \rangle^{\mathrm{T}} \tag{24}$$

where l_{IJ}^{edges} is the length of the element edge between nodes *I* and *J*, and $\hat{\boldsymbol{l}}_{IJ}^{edges}$ is direction cosine of the edge. Here the first term in the right hand side of the Eq. (22) means the conforming displacement of mid-edge point *K* expressed by corner rotations of nodes *I* and *J* in the edge-normal direction (Yunus *et al.* 1989), while the second term means the amplitude of the tangential non-conforming modes of mid-edge *K* in the edge-tantgential direction (Choi and Chung 1995).

Substituting the transformation given in Eq. (22) into Eq. (15) to yield the non-conventional interpolation for the displacement field.

$$\begin{aligned} \boldsymbol{u}^h = & \sum_{I=1}^{8} N_I^e(\xi,\ \eta,\ \zeta)\,\boldsymbol{u}_I^e + \sum_{K=9}^{20} N_K^{edges}(\xi,\ \eta,\ \zeta)\,\boldsymbol{T}_{IJ}^e(\boldsymbol{\psi}_I^e - \boldsymbol{\psi}_J^e) \\ & + \sum_{K=9}^{20} N_K^{edges}(\xi,\ \eta,\ \zeta)\,\hat{\boldsymbol{l}}_{IJ}^{edges}(\Delta\tilde{u}_K^{edges})_{tangential} \end{aligned} \tag{25}$$

Here, the number of the edge-tangential non-conforming displacements depends on the number of element edges. The non-conforming modes are applied only to the edge directions and there are 12 edge-tangential displacements in the 8-node solid element. Thus, the final non-conventional interpolation of displacement field in this study is arranged as follows

$$\boldsymbol{u}^h = \sum_{I=1}^{8}\left[N_I^e \boldsymbol{I} \;\middle|\; \sum_K N_K^{edges}\boldsymbol{T}_{IJ}^e\right]\begin{Bmatrix}\boldsymbol{u}_I^e \\ \boldsymbol{\psi}_I^e\end{Bmatrix} + \sum_{K=9}^{20} N_K^{edges}\hat{\boldsymbol{l}}_{IJ}^{edges}(\Delta\tilde{u}_K^{edges})_{tangential} \tag{26}$$

It is noted that instead of $(\boldsymbol{\psi}_I^e - \boldsymbol{\psi}_J^e)$ in Eq. (25), the corner rotation $\boldsymbol{\psi}_I^e$ is used in Eq. (26). This transformation can be done by summing up all the transformations with respect to the corner rotation $\boldsymbol{\psi}_I^e$, which meet at node *I*.

The proposed edge-tangential non-conforming modes was found to be the useful remedy for the Poisson's ratio locking caused by directionally varying displacement field within an element, since the edge-tangential parabolic non-conforming modes (Choi and Chung 1995) included in the displacement field (Eq. (26)) has the similar effect as natural space non-conforming tangential modes used by Yunus (Eq. (27)) to remedy the Poisson's ratio locking.

$$\begin{aligned} u_\xi^h &= (1-\xi^2)\tilde{u}_1^e \\ u_\eta^h &= (1-\eta^2)\tilde{u}_2^e \\ u_\zeta^h &= (1-\zeta^2)\tilde{u}_3^e \end{aligned} \tag{27}$$

Where u_ξ^h, u_η^h, u_ζ^h are interpolated non-conforming displacement in the natural ξ, η, ζ coordinate directions, respectively, and $\tilde{u}_1^e$, $\tilde{u}_2^e$, $\tilde{u}_3^e$ are scale factors, and the global strain tensors can be obtained from natural strain tensors by covariant tensor transformation

$$\bar{\varepsilon}_{ij}=\frac{\partial \xi_\alpha}{\partial x_i}\frac{\partial \xi_\beta}{\partial x_j}\varepsilon_{\alpha\beta} \tag{28}$$

Since conventional non-conforming modes are not adequate for this type of element because of existence of hierarchical shape functions which express nodal rotations, some other non-conforming modes as given as below are introduced to improve the general behavior of the brick type element (Choi and Chung 1995).

$$\begin{aligned}\bar{N}_1&=(1-\xi^2)(1-\eta^2)\\ \bar{N}_2&=(1-\eta^2)(1-\zeta^2)\end{aligned} \tag{29}$$

$$\begin{aligned}\bar{N}_3&=(1-\xi^2)(1-\zeta^2)\\ \bar{N}_4&=(1-\xi^2)(1-\eta^2)(1-\zeta^2)\end{aligned} \tag{30}$$

These are the form of the bubble functions in the two-dimensional and three-dimensional problems.

While displacement field is interpolated in a non-conventional fashion, the independent rotation field is interpolated in an isoparametric fashion.

$$\begin{pmatrix} u_4^h \\ u_5^h \\ u_6^h \end{pmatrix}=\begin{pmatrix} \psi_1^h \\ \psi_2^h \\ \psi_3^h \end{pmatrix}=\boldsymbol{\psi}^h=\sum_{I=1}^{8} N_I^e(\xi,\ \eta,\ \zeta)\,\boldsymbol{\psi}_I^e \tag{31}$$

The skew-symmetric stress field for the mixed type variational formulation is interpolated independently over each element. The interpolation of the skew-symmetric stress can be assumed as a linear polynomials given in the global coordinates. If skew-symmetric stress interpolation is defined with six parameters, $\boldsymbol{\beta}^e$, at the element level, then

$$skew\ \boldsymbol{\sigma}^h=\boldsymbol{S}^e\boldsymbol{\beta}^e \tag{32}$$

where

$$\boldsymbol{S}^e=\begin{bmatrix} 1 & \xi & & & & \\ & & 1 & \eta & & \\ & & & & 1 & \zeta \end{bmatrix} \tag{33}$$

To suppress spurious zero energy mode, adequate number of skew-symmetric interpolation parameters should be used for the element. With these six interpolation parameters, as defined above, the spurious zero energy mode can be suppressed successfully.

4. Element stiffness matrix

The infinitesimal strains can be defined from displacement field given in Eq. (26) as

$$symm\ \nabla \boldsymbol{u}^h=\sum_{I=1}^{8}(\boldsymbol{B}_I^e\boldsymbol{u}_I^e+\boldsymbol{G}_I^e\boldsymbol{\psi}_I^e)+\sum_{K=1}^{12}\boldsymbol{R}_K^e\Delta\tilde{\boldsymbol{u}}_K^e \tag{34}$$

where $\boldsymbol{u}_I^e$, $\boldsymbol{\psi}_I^e$, and $\Delta\tilde{\boldsymbol{u}}_K^e$ are, respectively, the nodal displacement, the nodal rotation, and the non-conforming displacement parameters in an element. Although several types of non-conforming modes or their combinations can be accommodated in this formulation, only the edge-

tangential non-conforming modes will be described here for simplicity. The strain-displacement and the strain-rotation matrix at node I are given follow:

$$\boldsymbol{B}_I^{eT}=\begin{bmatrix} N_{I,x}^e & & & N_{I,y}^e & & N_{I,z}^e \\ & N_{I,y}^e & & N_{I,x}^e & N_{I,z}^e & \\ & & N_{I,z}^e & & N_{I,y}^e & N_{I,x}^e \end{bmatrix} \quad I=1,\ 2,\ \cdots,\ 8 \tag{35}$$

$$\boldsymbol{G}_I^e=\sum_{edge}\boldsymbol{B}_K^{edges}\boldsymbol{T}_{IJ}^e \tag{36}$$

where, $\boldsymbol{B}_K^{edges}$ is the symmetric gradient of hierarchical shape functions N_K^{edges} in the form of Eq. (35), and $\boldsymbol{T}_{IJ}^e$ is the transformation matrix as given in Eq. (23). The symmetric gradient from the edge-tangential non-conforming displacement gives

$$\boldsymbol{R}_K^{eT}=\frac{1}{l_{IJ}^{edges}}\begin{bmatrix} \Delta x_{IJ}^e\widetilde{N}_{K,x}^{edges} \\ \Delta y_{IJ}^e\widetilde{N}_{K,y}^{edges} \\ \Delta z_{IJ}^e\widetilde{N}_{K,z}^{edges} \\ \Delta x_{IJ}^e\widetilde{N}_{K,y}^{edges}+\Delta y_{IJ}^e\widetilde{N}_{K,x}^{edges} \\ \Delta y_{IJ}^e\widetilde{N}_{K,z}^{edges}+\Delta z_{IJ}^e\widetilde{N}_{K,y}^{edges} \\ \Delta x_{IJ}^e\widetilde{N}_{K,z}^{edges}+\Delta z_{IJ}^e\widetilde{N}_{K,x}^{edges} \end{bmatrix} \quad K=1,\ 2,\ \cdots,\ 12 \tag{37}$$

where l_{IJ}^{edges} in the length of element edge joining nodes I and J, Δx_{IJ}^e, Δy_{IJ}^e and Δz_{IJ}^e are x, y and z components of the edge vector, respectively, which join nodes I and J in the global coordinate system, and $\widetilde{N}_K^{edges}$ is the edge-tangential non-conforming modes applied only to edge direction, which have the same shape functions as given in Eqs. (16), (17) and (18).

The discrete operator $\boldsymbol{G}_I^e$ and $\boldsymbol{R}_K^e$ need to be modified to avoid element locking. The modification fits into the framework of well-known $\bar{B}$-bar methods (Wilson, *et al.* 1990, 1991, Choi and Lee 1995) and reduces to changing strain-displacement matrices into

$$\bar{\boldsymbol{G}}^e=\boldsymbol{G}^e-\frac{1}{\Omega^e}\int_{\Omega^e}\boldsymbol{G}^e d\Omega \tag{38}$$

$$\bar{\boldsymbol{R}}^e=\boldsymbol{R}^e-\frac{1}{\Omega^e}\int_{\Omega^e}\boldsymbol{R}^e d\Omega \tag{39}$$

Furthermore, the infinitesimal rotation can be denoted similarly as

$$\begin{aligned} skew\ \nabla\boldsymbol{u}^h-\boldsymbol{\psi}^h=&\sum_{I=1}^{8}(\boldsymbol{A}_I^e\boldsymbol{u}_I^e+\boldsymbol{F}_I^e\boldsymbol{\psi}_I^e)+\sum_{K=1}^{12}\boldsymbol{Q}_K^e\Delta\widetilde{\boldsymbol{u}}_K^e-\sum_{I=1}^{8}N_I^e\boldsymbol{\psi}_I^e \\ &\sum_{I=1}^{8}(\boldsymbol{A}_I^e\boldsymbol{u}_I^e+\hat{\boldsymbol{F}}_I^e\boldsymbol{\psi}_I^e)+\sum_{K=1}^{12}\boldsymbol{Q}_K^e\Delta\widetilde{\boldsymbol{u}}_K^e \end{aligned} \tag{40}$$

where

$$\boldsymbol{A}_I^e=\frac{1}{2}\begin{bmatrix} 0 & -N_{I,z}^e & N_{I,y}^e \\ N_{I,z}^e & 0 & -N_{I,x}^e \\ -N_{I,y}^e & N_{I,x}^e & 0 \end{bmatrix} \quad I=1,\ 2,\ \cdots,\ 8 \tag{41}$$

$$\hat{\boldsymbol{F}}_I^e = \boldsymbol{F}_I^e - N_I^e \boldsymbol{I} \tag{42}$$

$$\boldsymbol{Q}_K^e = \frac{1}{2l_{IJ}^{edges}} \begin{bmatrix} \Delta z_{IJ}^e \widetilde{N}_{K,y}^{edges} - \Delta y_{IJ}^e \widetilde{N}_{K,z}^{edges} \\ \Delta x_{IJ}^e \widetilde{N}_{K,z}^{edges} - \Delta z_{IJ}^e \widetilde{N}_{K,x}^{edges} \\ \Delta y_{IJ}^e \widetilde{N}_{K,x}^{edges} - \Delta x_{IJ}^e \widetilde{N}_{K,y}^{edges} \end{bmatrix} \tag{43}$$

and $\boldsymbol{F}_I^e$ can be obtained by systematic transformation performed over all the edges which meet at node I

$$\boldsymbol{F}_I^e = \sum_{edge} \boldsymbol{A}_K^{edges} \boldsymbol{T}_{IJ}^e \tag{44}$$

Substituting Eqs. (34), (40) and (32) in Eq. (7), and minimizing the variational functional Π_γ for a single element, the equations can be written as

$$\begin{bmatrix} \boldsymbol{K}^e & \boldsymbol{H}^e \\ \boldsymbol{H}^{eT} & -\boldsymbol{V}^e \end{bmatrix} \begin{Bmatrix} \boldsymbol{a}^e \\ \boldsymbol{\beta}^e \end{Bmatrix} = \begin{Bmatrix} \boldsymbol{f}_{ext}^e \\ \boldsymbol{0} \end{Bmatrix}; \quad \boldsymbol{a}^e = \begin{Bmatrix} \boldsymbol{u}^e \\ \boldsymbol{\psi}^e \\ \Delta\widetilde{\boldsymbol{u}}^e \end{Bmatrix} \tag{45}$$

where

$$\boldsymbol{K}^e = \int_{\Omega^e} [\boldsymbol{B}^e \ \boldsymbol{G}^e \ \boldsymbol{R}^e]^T \boldsymbol{C} [\boldsymbol{B}^e \ \boldsymbol{G}^e \ \boldsymbol{R}^e] d\Omega \tag{46}$$

$$\boldsymbol{H}^{eT} = \int_{\Omega^e} \boldsymbol{S}^{eT} [\boldsymbol{A}^e \ \hat{\boldsymbol{F}}^e \ \boldsymbol{Q}^e] d\Omega \tag{47}$$

$$\boldsymbol{V}^e = \gamma^{-1} \int_{\Omega^e} \boldsymbol{S}^{eT} \boldsymbol{S}^e d\Omega \tag{48}$$

Since the skew-symmetric stress is interpolated independently in each element, the corresponding skew-symmetric parameters, $\boldsymbol{\beta}^e$, of the Eq. (45) may be eliminated at the element level through the static condensation. The non-conforming displacement, $\Delta\widetilde{\boldsymbol{u}}^e$, can also be eliminated in a similar manner, so that the remaining element global degrees of freedom are nodal displacements $\boldsymbol{u}^e$ and nodal rotations $\boldsymbol{\psi}^e$.

5. Numerical tests for validation of the elements

Several numerical tests were carried out to evaluate the validity and performance of the 8-node solid elements. A series of solid elements can be established by the selective use of different non-conforming modes. The elements with rotational degrees of freedom presented in this paper are denoted as

1. CHR : the element has no non-conforming modes.
2. NCH-1 : the element has four bubble-like non-conforming modes.
3. NCH-Y: the element have three natural space modes.
4. NCH-2 : the element include parabolic edge-tangential non-conforming modes.
5. NCH-3 : the element has both four bubble-like non-conforming modes and edge-tangential

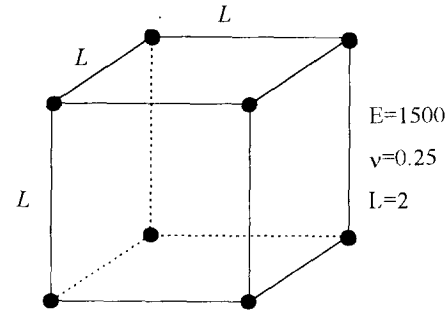

Fig. 7 Example for eigenvalue analysis.

Table 1 Number of zero eigenvalues for single unconstrained 8-node element for all presented element types

Element type	Number of eigenvalues	Number of zero eigenvalues	Number of spurious zero-energy modes
CHR	48	6	0
NCH-1	48	6	0
NCH-Y	48	6	0
NCH-2	48	6	0
NCH-3	48	6	0
NCH-4	48	6	0

non-conforming modes.

6. NCH-4: the element has both three natural space modes and bubble-like non-conforming modes.

where characters CH and NCH indicate the conforming hexahedron and non-conforming hexahedron, respectively. The elements used for comparison with the new elements in this study are NC-V1, C-V1 (Choi and Lee 1993) which are the non-conforming and conforming variable-node transition elements, respectively, and do not have any rotational degrees of freedom. In the numerical tests, the value of parameter γ is taken as the same value of shear modulus.

5.1. Eigenvalue analysis

To identify the possible spurious mechanicsms, eigenvalue analysis of the element matrix was carried out for the 8-node solid elements with rotational degrees of freedom. When mixed type formulation was used the number of skew symmetric stress parameters seems to be very important factor to stabilize the elements. If six skew-symmetric stress parameters are used, there are only six zero eigenvalues associated with rigid-body modes for the 8-node element shown Fig. 7, and no spurious mechanisms were expected to develop in any of the elements presented in this numerical test (See Table 1). If the number of stress parameters is not adequate, there may be the cases that the spurious zero energy modes can occur.

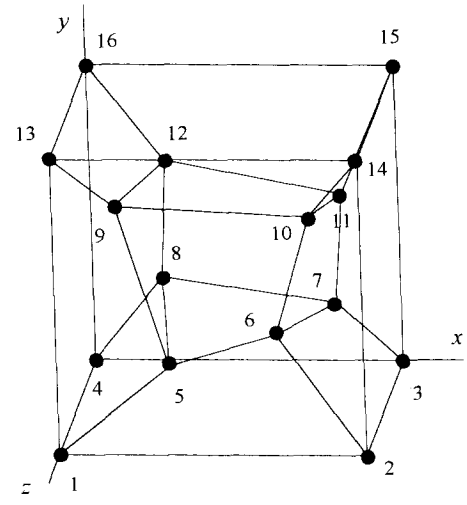

Fig. 8 Patch test model for 3D solid.

Table 2 Boundary condition and theoretical results

Boundary conditions	Theoretical solutions
$u=10^{-3}(2x+y+z)/2$	$\varepsilon_x=\varepsilon_y=\varepsilon_z=\gamma_{xy}=\gamma_{yz}=\gamma_{zx}=10^{-3}$
$v=10^{-3}(x+2y+z)/2$	$\sigma_x=\sigma_y=\sigma_z=2000$
$w=10^{-3}(x+y+2z)/2$	$\tau_{xy}=\tau_{yz}=\tau_{zx}=400$

5.2. Patch test

In order to check whether the proposed 8-node solid elements with rotational degrees of freedom are capable of representing constant strain states, the patch test was carried out. The typical test model is shown in Fig. 8 which contains distorted elements (Choi and Lee 1993, MacNeal and Harder 1985, Choi and Chung 1995). Problem was solved with the prescribed displacement boundary conditions and the obtained results are identical with the theoretical solutions for this problem (See Table 2).

5.3. Poisson's ratio locking test

To test for the Poisson's ratio locking, a single element under pure bending in plane strain boundary condition as shown in Fig. 9 is analyzed. The results for plane strain condifions are shown in Table 3. To check what type of non-conforming modes can prevent the Poisson's ratio locking, this test was carried out for an 8-node solid element with rotational degrees of freedom. It is evident from this test results that the tangential non-conforming modes are very effective for removal of the Poisson's ratio locking.

5.4. Cantilever beam under shear forces

To evaluate the general performance of the proposed element, a cantilever beam under shear

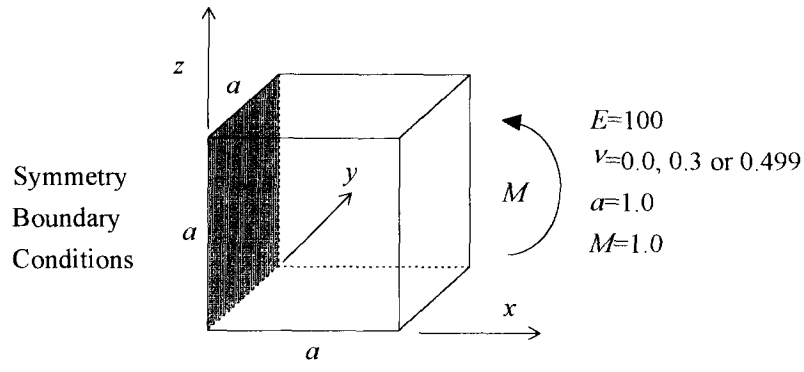

Fig. 9 Poisson's ratio locking test.

Table 3 Plane strain moment loading: relative accuracy of tip displacement

Element type	$\nu=0$	$\nu=0.3$	$\nu=0.499$
CHR	1.00	0.82	0.80
NCH-1	1.00	0.98	0.91
NCH-Y	1.00	1.00	1.00
NCH-2	1.00	1.00	1.00
NCH-3	1.00	1.00	1.00
NCH-4	1.00	1.00	1.00

forces at tip was tested. For this cantilever beams, the rotational boundary conditios for fastening end are symmetric on y-z plane, i.e. only the rotation about x axis is free to move. These rotational boundary conditions are consistent with those used for theoretical solutions. The test meshes which are composed of 8-node solid elements are shown in Fig. 10 ($E=1500$, $\nu=0.25$) along with the equivalent loads. But in this test, only translational forces are acted and uniformly distributed shear tractions are used. This may be the reason why resulting displacements are over the value of theoretical solutions.

The vertical displacements at A and the normal stress at B are presented in Tables 4 along with the theoretical results and the results obtained by different elements for the comparison. Here, it is shown that the proposed 8-node solid elements with rotational degrees of freedom give good result. In cases of highly distorted meshes, which are often occur in mesh gradation, the accuracy of results obtained by using elements with non-conforming modes are superior over those by conforming elements. In this numerical test, stress results are obtained from stress recovery method for non-conforming modes. The presented elements show improved results by the addition of non-conforming modes, among the elements, the elements designated as NCH-3 and NCH-4 showed the best results in performance.

5.5. Cantilever beam under pure bending

To evaluate the performance of the proposed element a cantilever beam uner a pure bending was tested. The rotational boundary conditions for fastening end are symmetric on y-z plane.

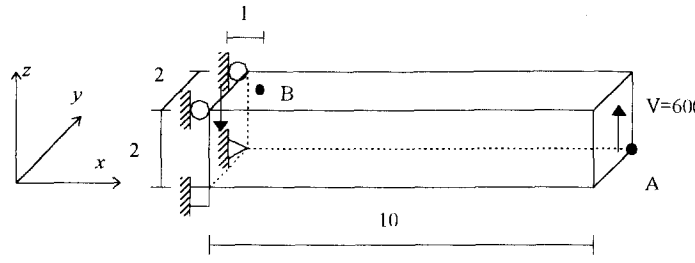

(a) Cantilever Beam under shear forces

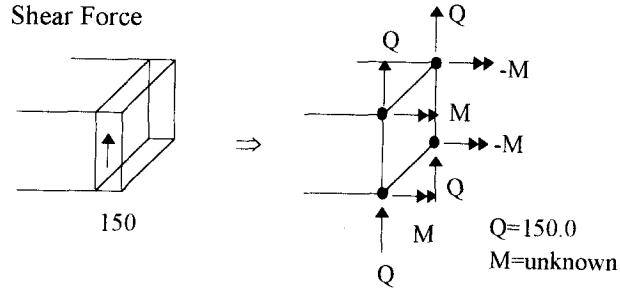

(b) Equivalent nodal forces including couples

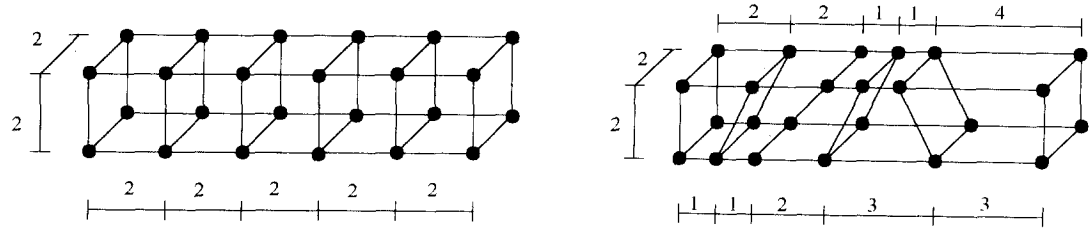

(c) Regular meshes (d) Distorted meshes

Fig. 10 Cantilever Beam under end tip shear force.

The test meshes are shown in Fig. 11 ($E=1500$, $\nu=0.25$) which are identical to the previous example. The equivalent nodal forces due to pure bending moment are shown in Fig. 11 for the 8-node solid element with rotational degrees of freedom.

The vertical displacements at A are presented in Tables 5 along with the theoretical results and those obtained by other elements for the comparison. Here, it is shown that the proposed 8-node solid elements with rotational degrees of freedom give good result. In cases of highly distorted meshes, the accuracy of results obtained by using elements with non-conforming modes are superior over those by conforming elements. The presented elements show improved results by the addition of non-conforming modes, among the elements, the elements designated as NCH-3 and NCH-4 showed the best in performance.

Table 4 Test results for cantilever beam under under tip shear force

Element	Mesh	Regular meshes			Distorted meshes		
		Point *A*		Point *B*	Point *A*		Point *B*
		Vertical displacement	Rotation about *y* axis	stress σ_{xx}	Vertical displacement	Rotation about *y* axis	stress σ_{xx}
C-V1 (Choi et al. 1995)		68.45	–	−2972.0	49.33	–	−2415.0
NC-V1 (Choi et al. 1995)		101.40	–	−4050.0	89.89	–	−3097.0
CHR		96.72	−14.30	−4091.0	83.62	−12.41	−3480.0
NCH-1		102.82	−15.29	−4145.0	91.85	−13.23	−3853.0
NCH-Y		103.02	−15.24	−4092.5	85.53	−12.88	−3991.0
NCH-2		103.04	−15.24	−4093.0	85.42	−12.63	−3949.5
NCH-3		103.11	−15.39	−4098.5	100.76	−15.62	−3158.5
NCH-4		103.10	−15.38	−4098.0	93.24	−14.37	−3840.5
Theory		102.625	−15.00	−4050.0	102.625	−15.00	−4050.0

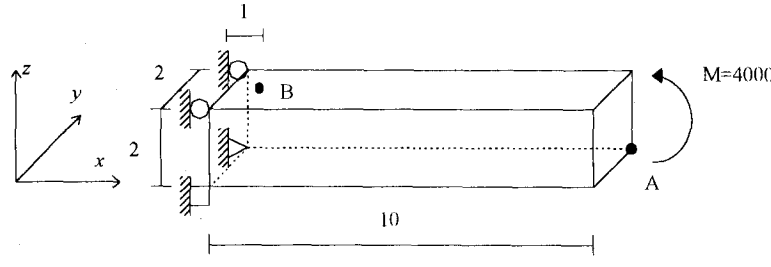

(a) Cantilever beam under pure bending

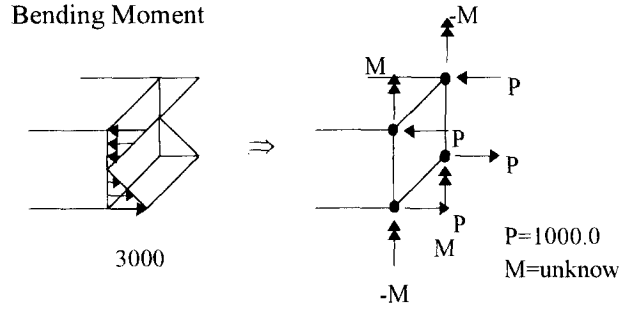

(b) Equivalent nodal forces including couples

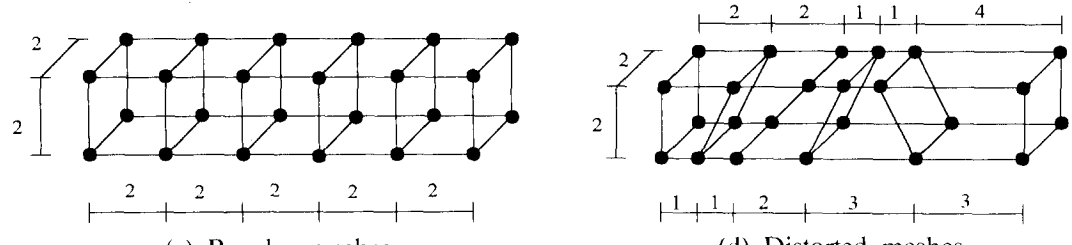

(c) Regular meshes (d) Distorted meshes

Fig. 11 Cantilever Beam under pure bending.

Table 5 Test results for cantilever beam under pure bending

Element \ Mesh	Regular meshes			Distorted meshes		
	Point *A*		Point *B*	Point *A*		Point *B*
	Vertical displacement	Rotation about *y* axis	stress σ_{xx}	Vertical displacement	Rotation about *y* axis	stress σ_{xx}
C-V1 (Choi et al. 1995)	66.67	–	−2200.0	44.38	–	−1736.0
NC-V1 (Choi et al. 1995)	100.00	–	−3000.0	87.45	–	−2262.0
CHR	93.75	−18.75	−3000.0	81.01	−16.80	−2432.0
NCH-1	99.70	−19.83	−3032.5	88.86	−17.15	−2824.0
NCH-Y	100.00	−20.00	−3000.0	84.24	−17.66	−2968.0
NCH-2	100.00	−20.00	−3000.0	82.64	−17.13	−2944.0
NCH-3	100.00	−20.00	−3000.0	97.33	−18.62	−2270.0
NCH-4	100.00	−20.00	−3000.0	91.75	−18.16	−2814.5
Theory	100.00	−20.00	−3000.0	100.00	−20.00	−3000.0

6. Conclusions

In this paper, 8-node solid elements with rotational degrees of freedom have been presented. The element is derived from the mixed variational principles which employs the independent rotational fields and employs skew-symmetric stress. The corner rotations are formulated by transforming the hierarchical mid-edge displacement that are a parabolic shape along an edge. A series of improved elements are obtained by selectively adding the non-conforming modes to the displacement fields.

It was found that addition of the tangential non-conforming modes to the non-conventional displacement fields eliminated the Poisson's locking phenomena which may appear under some plane strain boundary conditions.

It was verified that the proposed elements passed patch tests and caused no spurious zero energy mechanisms from the numerical tests. In 8-node solid element with rotational degrees of freedom, six skew-symmetric stress parameters were found to be sufficient for stability of the element. The presented new elements with non-conforming modes gave much improved results for the problems tested. Among the established elements, the elements designated as NCH-3 and NCH-4 produced the best performances.

The 3D element with rotational degrees of freedom can be effectively applied to the practical structural problems due to its simplicity in modeling and improved performance. The more intensive study on the application of this element will follow in the future studies.

References

Allman, D.J. (1984), "A compatible triangular element including vertex rotations for plane elasticity analysis", *Comp. and Struct.* **19**(2), 1-9.

Allman, D.J. (1984), "A compatible triangular element including vertex rotations for plane elasticity analysis", *Comp. Struct.* **19**(1-2), 1-8.

Allman, D.J. (1988), "A quadrilateral finite element including vertex rotations for plane elasticity problem", *Int. J. Numer. Methods Eng.*, **26**, 717-739.

Choi, C.K. and Lee, N.H. (1993), "Three dimensional solid elements for adaptive mesh gradation", *Structural Engineering and Mechanics*, **1**(1), 61-74.

Choi, C.K. and Lee, W.H. (1995), "Transition membrane elements with drilling freedom for local mesh refinements", *Structural Engineering and Mechanics*, **3**(1), 75-89.

Choi, C.K. and Chung, K.Y. (1995), "Three dimensional variable node solid element with drilling degrees of freedom", *Proceedings of 6th International Conference on Computing in Civil and Building Eng.*, Berlin, Germany, 12-15 July, **1**, 521-528.

Cook, R.D. (1986), "On the allman triangle and related quadrilateral element", *Comp. Struct*, **22**(6), 1065-1067.

Cook, R.D. (1987), "A plane hybrid element with rotational D.O.F. and adjustable stiffiness", *Int. J. Numer. Methods Eng.*, **24**, 1499-1500.

Hughes, T.J.R. and Brezzi, F. (1989), "On drilling degrees of freedom", *Comp. Methods Appl. Mech. Eng.* **72**, 105-121.

Ibrahimbegovic, A. and Wilson, E.L. (1991), "Thick shell and solid finite elements with independent rotation fields", *Int. J. Numer. Methods Eng.*, **31**, 1393-1414.

Ibrahimbegovic, A. and Wilson, E.L. (1991), "A modified method of incompatible modes", *Communications in applied Numerical Methods*, **7**, 187-194.

Ibrahimbegovic, A. and Wilson, E.L. (1991), "A modified mothod of incompatible modes", *Communications in applied Numerical Methods*, **7**, 187-194.

Irons, B. and Ahmad, S. (1980), *Techniques of Finite Elements*, Ellis Horwood, Chichester, U.K.

MacNeal, R.H. and Harder, R.LO. (1985), "A proposed standard set of problems to test finite element accuracy", *Finite Elements in Analysis and Design*, **1**, 3-20.

MacNeal Richard, H. and Harder Robert, L. (1988), "A refined four-noded membrane element with rotational degrees of freedom", *Comp. Struct.* **28**(1), 75-84.

Pawlak, Timothy P., Yunus, Shah M. and Cook, R.D. (1991), "Solid elements with rotational degrees of freedom: part II-tetrahedron elements", *Int. J. Numer. Methods Eng.*, **31**, 593-610.

Reissner, E. (1965), "A note on variational theorems in elasticity", *Int. J. solids and Structures*, **1**, 93-95.

Timoshenko, S. and Goodier, J.N. (1951), *Theory of Elasticity*, McGraw-Hill, New York.

Wilson, E.L. and Ibrahimvegovic Adnan (1990), "Use of incompatible displacement modes for calculation of element stiffness or stresses", *Finite Element in Analysis and Design*, **7**, 229-241.

Yunus, Shah M., Pawlak, Timothy P. and Cook, R.D. (1991), "Solid elements with rotational degrees of freedom: part I-hexahedron elements", *Int. J. Numer. Methods Eng.*, **31**, 573-592.

Yunus, Shah M., Saigal Sunil and Cook, Robert, D. (1989), "On improved hybrid finite elements with rotational degrees of freedom", *Int. J. Numer. Methods Eng.*, **28**, 785-800.